Chaotic Modeling and Simulation (CMSIM) 3: 269-283, 2018

The FitzHugh-Nagumo Model and 2-D Solvable Chaos Maps

Shunji Kawamoto

Osaka Prefecture University, Sakai, Osaka, Japan
(E-mail: kawamoto@eis.osakafu-u.ac.jp)

Abstract. It is shown firstly that the forced Van der Pol oscillator and the forced Duffing oscillator are transformed into two-dimensional (2-D) models by a commonly used transformation and/or the Liénard transformation, and the 2-D models are compared with the FitzHugh-Nagumo (FHN) model, which explains neural phenomena. Then, the related 2-D solvable chaos maps to the FHN model are derived from the 2-D chaos solutions, and the solutions corresponding to the orbit of neural cells are numerically calculated with the algorithm and a MATLAB program. Finally, the mean free time, the particle-like and the wavefront-like properties of orbit, and the dynamic stability region for neural cells are briefly discussed on the basis of the numerical result.
Keywords: Van der Pol oscillator, Duffing oscillator, Liénard transformation, FitzHugh-Nagumo model, 2-D solvable chaos map, Mean free time, Particle-like property, Wavefront-like property, Dynamic stability region.

1 Introduction

Over a long period, papers and books on nonlinear dynamics have appeared in order to describe the nonlinear science [1, 2]. As is well discussed, nonlinear difference equations and differential equations have arisen widely in the field of biological, physical, chemical, mechanical, electrical and social sciences, and are known to possess a rich spectrum of dynamical behavior as chaos in many respects [3-6]. In the meantime, scientists, mathematicians and engineers have come to understand the complicated behavior and the fundamentals of chaos [7, 8]. Particularly, a population growth in biology has been afforded by the simplest nonlinear difference equation called the logistic map, which is analogous to the logistic function and equation [9]. After many attempts, a piecewise-linear electric circuit is accepted to generate chaos [10], and various chaotic sequences have been proposed for pseudo-random numbers and cryptosystems [11-13].

On the other hand, for biological systems, a mathematical model to explain the electrical behavior through the surface membrane of squid giant axons has been presented [14], and impulse trains in the model have been considered by the phase space methods and the equivalent electric circuit as one of a large class of nonlinear systems, which show excitable and oscillatory behaviors [15, 16]. In addition, dynamic experiments have been performed for the evidence of chaotic

Received: 29 October 2017 / Accepted: 26 March 2018

ISSN 2241-0503

behaviors of the giant neuron in marine mollusk, and the chaotic field potential of rat hippocampus is recorded by using microelectrodes [17, 18].
Recently, chaos functions and its application to engineering have been proposed, and one-dimensional (1-D), 2-D and 3-D solvable chaos maps are derived from the chaos solutions [19, 20]. The aim of this paper is firstly to show in Section 2 that the forced Van der Pol oscillator [21] and the forced Duffing oscillator [22, 23] are transformed into 2-D models, and are compared with the FitzHugh-Nagumo (FHN) model [15, 16] for neural phenomena. Secondly, 2-D solvable chaos maps corresponding to the FHN model are derived in Section 3. Finally, Section 4 is devoted to the numerical calculation with the algorithm and a MATLAB program. In addition, from the numerical result, the mean free time, the particle-like and the wavefront-like properties of orbit, and the dynamic stability region for neural cells are briefly discussed. Conclusions are summarized in the last Section.

2 The FitzHugh-Nagumo Model

For nonlinear differential equations of the second order, we consider firstly the forced Van der Pol oscillator [21] given by

$$\ddot{x} - \varepsilon(1 - x^2)\dot{x} + x = E_0 \sin(\omega t), \tag{1}$$

which represents a model for a simple vacuum tube oscillator circuit with a nonlinear damping term, where $x = x(t)$ is the proposition coordinate function of time *t*, and $\{\varepsilon \neq 0,\ E_0,\ \omega\}$ are the system parameters. By a commonly used transformation $y \equiv \dot{x}$, we have the following 2-D model from (1) as

$$\dot{x} = y, \tag{2}$$
$$\dot{y} = \varepsilon(1 - x^2)y - x + E_0 \sin(\omega t), \tag{3}$$

where the term $E_0 \sin(\omega t)$ in (3) is the external force of (1). Moreover, by the Liénard transformation [15];

$$y \equiv x - \frac{1}{3}x^3 - \frac{1}{\varepsilon}\dot{x}, \tag{4}$$

we find another 2-D model from (1) and (4) as

$$\dot{x} = \varepsilon(x - \frac{1}{3}x^3 - y), \tag{5}$$
$$\dot{y} = \frac{1}{\varepsilon}x - \frac{1}{\varepsilon}E_0 \sin(\omega t), \tag{6}$$

which is known to have chaotic behaviors in the equivalent circuit with sinusoidal forcing [24].
Secondly, we discuss the forced Duffing oscillator of the form;

$$\ddot{x} + \delta\dot{x} + \alpha x + \beta x^3 = \gamma \cos(\omega t), \tag{7}$$

where $x = x(t)$ is the displacement at time t, $\dot{x}$ is the velosity, and $\ddot{x}$ is the acceleration. The coefficients $\{\alpha, \beta, \gamma, \delta\}$ are real constants, and the rhs of (7) gives a periodic driving force. Here, it is well known that randam oscillations occuring in the equivalent nonlinear electric circuit to (7), have been studied, and the points of orbit give the Japanese attractor on the phase-plane [22, 23]. By the commonly used transformation $y \equiv \dot{x}$, the differential equation (7) is rewritten into a 2-D model as

$$\dot{x} = y, \tag{8}$$

$$\dot{y} = -\alpha x - \beta x^3 - \delta y + \gamma \cos(\omega t), \tag{9}$$

which has a similar form to the 2-D model (2) and (3) of the forced Van der Pol oscillator (1), and has the third-order nonlinear term in (9).
On the other hand, the FitzHugh-Nagumo (FHN) model [15, 16] is a 2-D simplification of the Hodgkin-Huxley model [14] of spike generation in squid giant axons, and is given by

$$\dot{v} = v - \frac{1}{3}v^3 - w + I(t), \tag{10}$$

$$\dot{w} = \frac{1}{\tau}(v + a - bw), \tag{11}$$

which has an electric circuit for (10) and (11) as one of a large class of nonlinear systems showing excitable and oscillatory behaviors, where v is the membrane potential, w is the recovery variable, $I(t)$ is the stimulus external current, and $\{a,\ b,\ \tau \neq 0\}$ are model parameters. Here, it is interesting to note that the forced Van der Pol oscillator (1) has an equivalent circuit involving the tunnel-diode to the FHN model (10) and (11) [16, 24]. Moreover, it should be noticed that the 2-D model (5) and (6) of the forced Van der Pol oscillator has the external voltage term in (6), and the FHN model (10) and (11) has the stimulus external current term in (10).

3 2-D Solvable Chaos Maps

We have derived 2-D models of the forced Van der Pol oscillator and the forced Duffing oscillator in Section 2, and have compared the models with the FHN model, which explains neural phenomena. In this Section, 2-D solvable chaos maps are derived, and are discussed by introducing the proposed time-dependent chaos functions [19, 20].

Firstly, from the following chaos solutions consisting of time-dependent chaos functions;

$$x_n(t) = a_1 \sin^2(2^n t) + b_1, \tag{12}$$

$$y_n(t) = a_2 \cos(2^n t) + b_2, \tag{13}$$

with $$t \neq \pm m\pi / 2^l, \tag{14}$$

here $\{a_1 \neq 0, a_2 \neq 0, b_1, b_2\}$ are coefficients and parameters, $\{l, m\}$ are finite positive integers, and the condition obtained from (12) and (13) is

$$\frac{1}{a_1}(x_n(t) - b_1) + \frac{1}{a_2^2}(y_n(t) - b_2)^2 = 1, \tag{15}$$

then we have a 2-D solvable chaos map as

$$x_{n+1}(t) = \frac{4}{a_2^2}(x_n(t) - b_1)(y_n(t) - b_2)^2 + b_1, \tag{16}$$

$$y_{n+1}(t) = -(\frac{2a_2}{a_1})x_n(t) + (a_2 + b_2 + \frac{2a_2 b_1}{a_1}), \tag{17}$$

which has chaos solutions (12) and (13) with (14), and therefore we find that the form of the 2-D map (16) and (17) corresponds to the 2-D model (5) and (6) of the forced Van der Pol oscillator, and to the FHN model (10) and (11). The third-order nonlinear term is involved in (5), (10) and (16), respectively.

Secondly, from the chaos solutions consisting of the same time-dependent chaos functions as (12) and (13) given by, in the reverse order of chaos functions;

$$x_n(t) = a_1 \cos(2^n t) + b_1, \tag{18}$$

$$y_n(t) = a_2 \sin^2(2^n t) + b_2, \tag{19}$$

with (14) and the following condition obtained from (18) and (19);

$$\frac{1}{a_1^2}(x_n(t) - b_1)^2 + \frac{1}{a_2}(y_n(t) - b_2) = 1, \tag{20}$$

then we derive another 2-D solvable chaos map as

$$x_{n+1}(t) = -(\frac{2a_1}{a_2})y_n(t) + (a_1 + b_1 + \frac{2a_1 b_2}{a_2}), \tag{21}$$

$$y_{n+1}(t) = \frac{4}{a_1^2}(x_n(t)-b_1)^2(y_n(t)-b_2)+b_2, \tag{22}$$

which has chaos solutions (18) and (19) with (14). Here, the form of the 2-D map (21) and (22) corresponds to the 2-D model (2) and (3) of the forced Van der Pol oscillator (1), and to the 2-D model (8) and (9) of the forced Duffing oscillator (7). Therefore, it is interesting to note that the 2-D model (2) and (3) of the forced Van der Pol oscillator is equivalent to the 2-D model (8) and (9) of the forced Duffing oscillator, in terms of replacing the coodinate axis with chaos functions from (12) and (13) to (18) and (19).

4 Numerical Calculation

In general, computer simulation and physical experiment are the most widely used techniques for understanding dynamical behaviors in chaotic systems. In this Section, chaos solutions (12)-(14) to the 2-D solvable chaos map (16) and (17) are numerically simulated, and the properties are discussed.

It is important to emphasize that if we regard the parameter b_1 in (12) as a function of time $b_1 = b_1(t)$, and $b_2 = 0$ for simplicity, then the solutions (12)-(14), the condition (15) and the 2-D chaos map (16) and (17) are rewritten as

$$x_n(t_i) = a_1 \sin^2(2^n t_i) + b_1(t_i), \tag{23}$$

$$y_n(t_i) = a_2 \cos(2^n t_i), \tag{24}$$

$$\frac{1}{a_1}(x_n(t_i)-b_1(t_i)) + \frac{1}{a_2^2} y_n^{\,2}(t_i) = 1, \tag{25}$$

$$x_{n+1}(t_i) = \frac{4}{a_2^2}(x_n(t_i)-b_1(t_i)) y_n^{\,2}(t_i) + b_1(t_i), \tag{26}$$

$$y_{n+1}(t_i) = -(\frac{2a_2}{a_1})x_n(t_i) + a_2 + (\frac{2a_2}{a_1})b_1(t_i), \tag{27}$$

where we choose a discrete time $t = t_i$ satisfying (14). Therefore, the $b_1(t_i)$ in (26) corresponds to the stimulus external current $I(t)$ of the FHN model (10) and (11), and the term $(2a_2/a_1)b_1(t_i)$ in (27) is corresponding to the external force $E_0 \sin(\omega t)$ of the 2-D model (5) and (6) for the forced Van der Pol oscillator, respectively.

Thus, we calculate numerically the chaos solutions (23) and (24) by introducing the following algorithm for long time chaotic series to avoid the accumulation of round-off error caused by the numerical iteration of (23) and (24);

$$
\begin{aligned}
& i = 0,1,2,3,\ldots, N, \\
& n = 0,1,2,3,\ldots, N, \\
& t_i = i(\Delta t) = 0, \Delta t, 2(\Delta t), 3(\Delta t), \ldots, N(\Delta t), \\
& \Delta t = t_{i+1} - t_i = (l_0 / p_r)\pi, \\
& i:\ \ x_n(t_i) = \sin^2(2^n t_i) \\
& \qquad\qquad = \sin^2(2^n i(\Delta t)) \\
& \qquad\qquad = \sin^2(2^n l_0 (i / p_r)\pi) \\
& \qquad\qquad \equiv \sin^2(l_n (i / p_r)\pi), \\
& \qquad\quad l_n i \equiv \mathrm{mod}(2 l_{n-1} i, p_r), \\
& \quad y_n(t_i) \equiv \cos(l_n (i / p_r)\pi), \\
& \qquad\quad l_n i \equiv \mathrm{mod}(2 l_{n-1} i, 2 p_r), \\
& i+1:\ \ x_n(t_{i+1}) \equiv \sin^2(l_n((i+1) / p_r)\pi), \\
& \qquad l_n(i+1) \equiv \mathrm{mod}(2 l_{n-1}(i+1), p_r), \\
& \qquad y_n(t_{i+1}) \equiv \cos(l_n((i+1) / p_r)\pi), \\
& \qquad l_n(i+1) \equiv \mathrm{mod}(2 l_{n-1}(i+1), 2 p_r), \\
& i+2:\ \cdots
\end{aligned}
\tag{28}
$$

where N is the iteration number, (l_0 / p_r) is a rational number, l_0 is the initial integer of l_n, and p_r is a large prime number [20, 25].

In Fig. 1, it is illustrated that the mean free time Δt given in the algorithm (28) is the average time of a neural cell travel between two collision points $(x_n(t_i), y_n(t_i))$ and $(x_{n+1}(t_{i+1}), y_{n+1}(t_{i+1}))$ with other cells of the orbit on the $x_n - y_n$ plane, as a chaotic process. Therefore, it should be noted that the time Δt is changeable by setting the rational number (l_0 / p_r) for each travel in the algorithm (28).

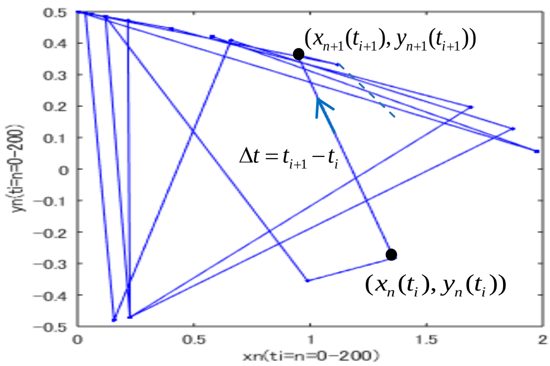

Fig. 1. The mean free time Δt between two collision points of the orbit.

The numerical results are shown in Figs. 2-5 for the orbit of one neural cell with initial values $\{x_0 = x_{n=0}(t_{i=0}), y_0 = y_{n=0}(t_{i=0})\}$; (a) the external force $b_1(t_i)$ in (23) corresponding to the stimulus external current of the FHN model, (b) the membrane potential $x_n(t_i)$, (c) the recovery variable $y_n(t_i)$, and (d) the orbit on the $x_n - y_n$ plane, in Figs. 2-5. For the calculation, the term $b_1(t_i)$ is given as an input signal, and the iteration number is *N*=200. Then, we choose the prime number $p_r = 431$ in (28), according to $p_r \geq 2N+1$, in order to avoid the accumulation of round-off error and the periodicity caused by the iteration [25]. For reference, a MATLAB program for Fig. 3 is given in Appendix.

Next, in Fig. 2(a)-(d), the external force $b_1(t_i)$ with no pulse in (a), the chaos solution $x_n(t_i)$ (23) with $a_1 = 2.0$ in (b), another solution $y_n(t_i)$ (24) with $a_2 = 0.5$ in (c), and the orbit of one neural cell on the $x_n - y_n$ plane with an initial point $(x_0, y_0) = (0, a_2 = 0.5)$ for (23) and (24) in (d), are illustrated, respectively. Here, it is found that $x_n(t_i)$ in (b) and $y_n(t_i)$ in (c) give chaotic time series, and have a particle-like property. However, all the collision points of orbit in (d) are on the discrete quadratic curve given by the condition (25), and show a wavefront-like property on the $x_n - y_n$ plane. In addition, it is interesting to note that the strange attractor of the Hénon map [26] has a similar discrete curve to Fig. 2(d).

In Figs. 3-5, chaos solutions $x_n(t_i)$ and $y_n(t_i)$ are shown in (b) and (c) for the cases that rectangular pulses of $b_1(t_i)$ in (a) are forced as an input signal. One pulse input $b_1(t_i)$ in Fig. 3(a), two pulse input in Fig. 4(a), and two (positive and negative) pulse input in Fig. 5(a) are presented. In Figs. 3(b), 4(b) and 5(b), chaotic time series responding to each pulse input $b_1(t_i)$ are obtained by calculating (23). It is important here to notice that the similar chaotic responses to Figs. 3(b)-5(b) are experimentally recorded for the giant neuron of marine mollusk and the rat hippocampus [17, 18]. Then, for the $x_n - y_n$ plane of Figs. 3(d)-5(d), the orbit of one neural cell is found to be on the discrete quadratic curve (25), and the neural cell is pushed forward from the wavefront-like curve onto another discrete curve by the discrete pulse input signal $b_1(t_i)$, as a signal propagation. Thus, the neural cell is pushed forward and/or backward depending on the input signal $b_1(t_i)$ as illustrated in Figs. 3(d)-5(d). Therefore, the 2-D system (23)-(27) for neural cells may describe a physics of non-equilibrium open systems.

Generally, fixed points and the linear stability for a given nonlinear difference equation are commonly studied in order to determine the stability. However, for the case of the 2-D solvable chaos map (26) and (27), which is derived from the solutions (23) and (24), we have the condition (25) consisting of chaos solutions (23) and (24), and the orbit starting from the initial point $(x_0, y_0) = (0, a_2 = 0.5)$ of

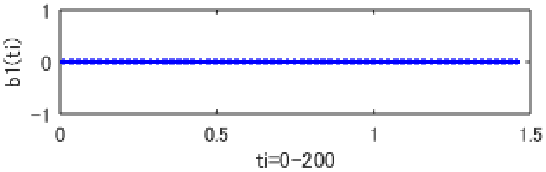

(a) $b_1(t_i)$

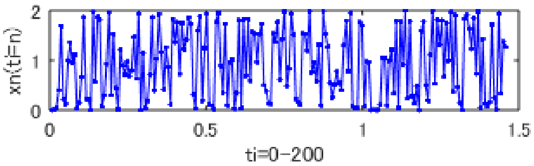

(b) $x_n(t_i)$

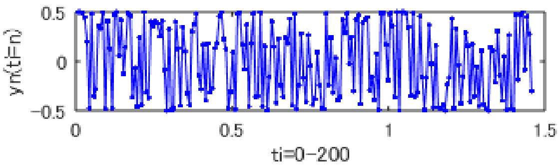

(c) $y_n(t_i)$

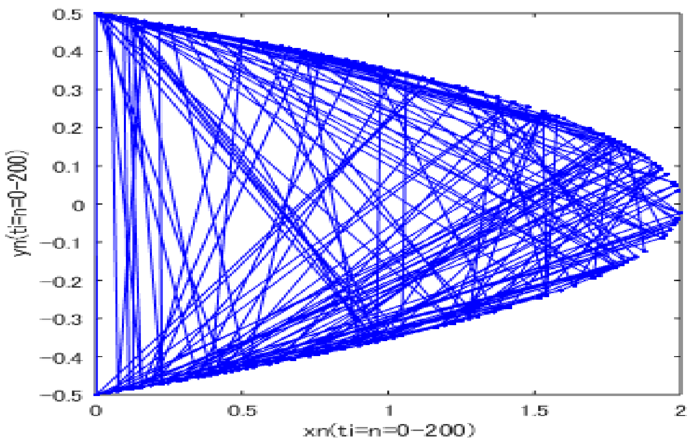

(d) $x_n - y_n$

Fig. 2. No pulse input $b_1(t_i)$, chaotic time series $x_n(t_i)$, $y_n(t_i)$ and the $x_n - y_n$ plane.

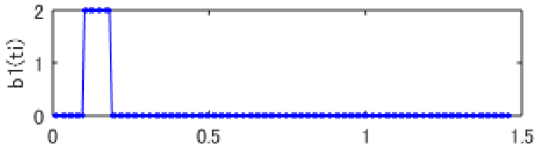

(a) $b_1(t_i)$

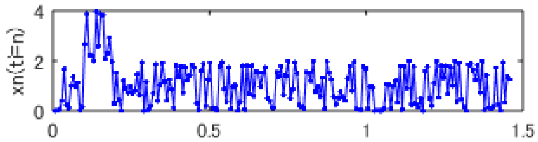

(b) $x_n(t_i)$

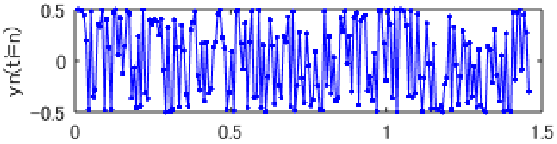

(c) $y_n(t_i)$

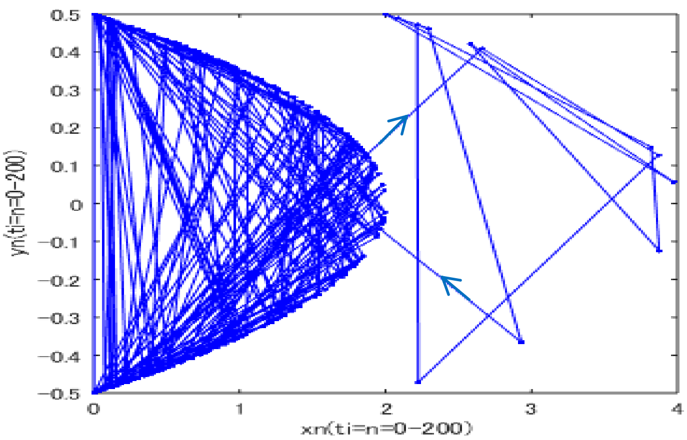

(d) $x_n - y_n$

Fig. 3. One pulse input $b_1(t_i)$, chaotic time series $x_n(t_i)$, $y_n(t_i)$ and the $x_n - y_n$ plane.

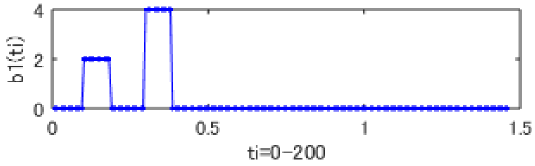

(a) $b_1(t_i)$

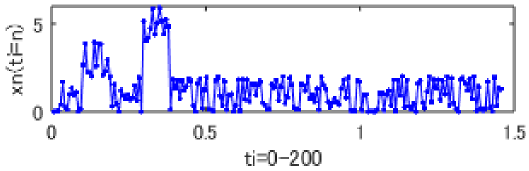

(b) $x_n(t_i)$

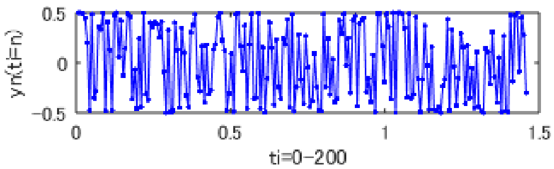

(c) $y_n(t_i)$

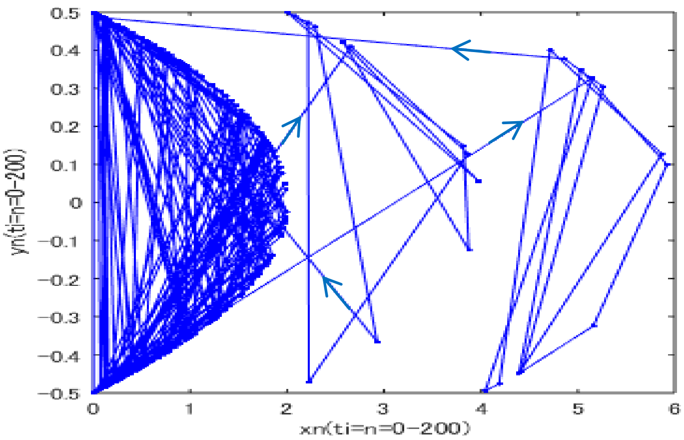

(d) $x_n - y_n$

Fig. 4. Two pulse input $b_1(t_i)$, chaotic time series $x_n(t_i)$, $y_n(t_i)$ and the $x_n - y_n$ plane.

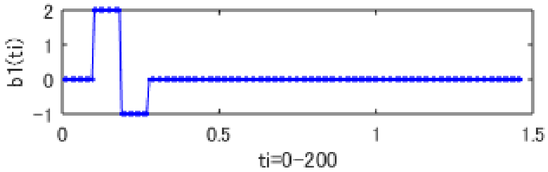

(a) $b_1(t_i)$

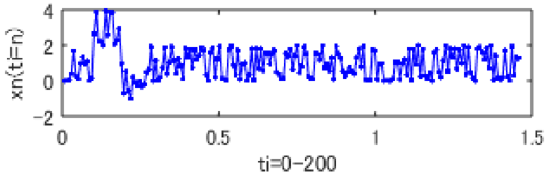

(b) $x_n(t_i)$

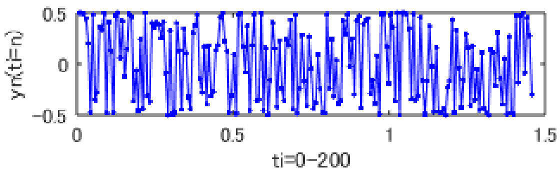

(c) $y_n(t_i)$

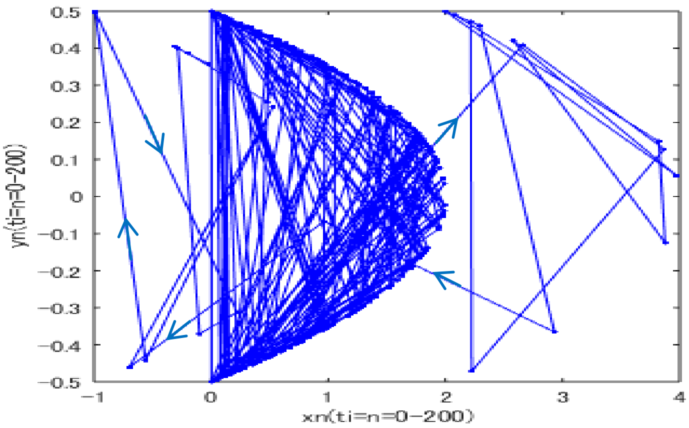

(d) $x_n - y_n$

Fig. 5. Two (positive and negative) pulse input $b_1(t_i)$, chaotic time series $x_n(t_i)$, $y_n(t_i)$ and the $x_n - y_n$ plane.

the solutions (23) and (24) has a discrete dynamic stability region given by

$$\frac{1}{a_1}(x_n(t_i) - b_1(t_i)) + \frac{1}{a_2^{\,2}} y_n^{\,2}(t_i) \le 1, \tag{29}$$

which is numerically obtained by iterating the map (26) and (27), and relates to the fractal sets for nonlinear dynamics of the 2-D chaotic maps, as considered in [27].

Conclusions

As a result, we find in Sections 2 and 3 that 2-D models of the forced Van der Pol oscillator and the forced Duffing oscillator are equivalent to the FHN model from a viewpoint of the 2-D chaos solutions with the external force $b_1(t_i)$. Then, we have calculated the solutions (23) and (24) numerically with the algorithm and a MATLAB program, and finally have discussed in Section 4 that the mean free time Δt, the particle-like property, the wavefront-like property and the dynamic stability region based on the quadratic curve (25) with the discrete function of time $b_1(t_i)$ as an input signal, would be helpful for describing the chaotic dynamics of neural cells in real neural phenomena.

Appendix

```
% MATLAB program for Fig. 3 by S. Kawamoto
% initial conditions
T=zeros (1,200);
B1=zeros (1,200);
ILN1=zeros (200,200);
ILN2=zeros (200,200);
X=zeros (200,200);
Y=zeros (200,200);
XX=zeros (1,200);
YY=zeros (1,200);
L=1;
PR=431;
A1=2.0;
A2=0.5;
% external input b1(ti) and 2-D chaos solutions
for I=1:200, T(I)=I.*L.*pi./PR; end
for I=1:13, B1(I)=0.0; end
for I=14:25, B1(I)=2.0; end
for I=26:200, B1(I)=0.0; end
for I=1:200
    for N=1
        ILN1(I,N)=mod(2ˆN.*I.*L,PR);
        X(I,N)=A1.*(sin(ILN1(I,N).*pi./PR)).ˆ2+B1(I);
        ILN2(I,N)=mod(2ˆN.*I.*L,2*PR);
```

```
        Y(I,N)=A2.*cos(ILN2(I,N).*pi./PR);
    end
    for N=2:I
        ILN1(I,N)=mod(2.*ILN1(I,N-1),PR);
        X(I,N)=A1.*(sin(ILN1(I,N).*pi./PR)).ˆ2+B1(I);
        ILN2(I,N)=mod(2.*ILN2(I,N-1),2*PR);
        Y(I,N)=A2.*cos(ILN2(I,N).*pi./PR);
    end
end
for I=1:200
    XX(I)=X(I,I);
      YY(I)=Y(I,I);
end
% figures (a)-(d)
figure('position',[100 100 350 100])
plot(T,B1,'-b.','MarkerFaceColor','b','MarkerSize',7);
xlabel('ti=0-200'); ylabel('b1(ti)')
figure('position',[100 100 350 100])
plot(T,XX,'-b.','MarkerFaceColor','b','MarkerSize',7);
xlabel('ti=0-200'); ylabel('xn(ti)')
figure('position',[100 100 350 100])
plot(T,YY,'-b.','MarkerFaceColor','b','MarkerSize',7);
xlabel('ti=0-200'); ylabel('yn(ti)')
figure('position',[100 100 350 350])
plot(XX,YY,'-b.','MarkerFaceColor','b','MarkerSize',7);
xlabel('xn(ti=0-200)'); ylabel('yn(ti=0-200)')
```

References

1. E. A. Jackson. *Perspectives of Nonlinear Dynamics*. Cambridge University Press, Cambridge, 1989.
2. A. Scott. *Nonlinear Science*. Routledge, London, 2005.
3. R. M. May. Biological populations with non-overlapping generations: Stable points, stable cycles, and chaos. *Science* 15: 645-646, 1974.
4. T. Y. Li and J. A. Yorke. Period three implies chaos. *American Mathematics Monthly* 82: 985-992, 1975.
5. R. M. May. Simple mathematical models with very complicated dynamics. *Nature* 261: 459-467, 1976.
6. F. C. Moon. *Chaotic and Fractal Dynamics*. Wiley, New York, 1992.
7. E. Ott. *Chaos in Dynamical Systems*. Cambridge University Press, Cambridge, 1993.
8. S. H. Strogatz. *Nonlinear Dynamics and Chaos*. Westview Press, Boulder, 1994.
9. P. F. Verhulst. Mathematical researches into the law of population growth increase. *Nouveaux Mémoires de l'Académie Royale des Sciences et Belles–Lettres de Bruxelles* 18: 1-42, 1845.
10. L. O. Chua, C. A. Desoer and E. S. Kuh. *Linear and Nonlinear Circuits*. McGraw-Hill, New York, 1987.
11. L. M. Pecora and T. L. Carroll. Synchronization in chaos systems. *Phys. Rev. Lett.* 64: 821-824, 1990.
12. G. Perez and H. A. Cerdeira. Extracting message masked by chaos. *Phys. Rev. Lett.* 74: 1970-1973, 1995.

13. G. D. V. Wiggeren and R. Roy. Optical communication with chaotic waveforms. *Phys. Rev. Lett.* 81: 3547-3550, 1998.
14. A. L. Hodgkin and A. F. Huxley. A quantitative description of membrane current and its application to conduction and excitation in nerve. *J. Physiol*. 117: 500-544, 1952.
15. R. FitzHugh. Impulses and physiological states in theoretical models of nerve membrane. *Biophysical Journal* 1: 445-466, 1961.
16. J. Nagumo, S. Arimoto and S. Yoshizawa. An active pulse transmission line simulating nerve axon. *Proc. IRE*. 50: 2061-2070, 1962.
17. H. Hayashi, S. Ishizuka, M. Ohta and K. Hirokawa. Chaotic behaviour in the Onchidium giant neuron under sinusoidal simulation. *Phys. Lett*. 88A: 435-438, 1982.
18. H. Hayashi and S. Ishizuka. Chaotic responses of the hippocampal CA3 region to a mossy fiber stimulation in vitro. *Brain Res*. 686: 194-206, 1995.
19. S. Kawamoto. 2-D and 3-D solvable chaos maps. *Chaotic Modelling and Simulation (CMSIM)* 1: 107-118, 2017.
20. S. Kawamoto. Chaotic time series by time-discretization of periodic functions and its application to engineering. *Chaotic Modelling and Simulation (CMSIM)* 2: 193-204, 2017.
21. B. Van der Pol and J. Van der Mark. Frequency demultiplication. *Nature* 120 (3019): 363-364, 1927.
22. Y. Ueda. Random phenomena resulting from nonlinearity: In the system described by Duffing's equation. *Int. J. Non-linear Mechanics* 20: 481-491, 1985: Translated from *Trans. IEEJ* 98-A: 167-173, 1978.
23. Y. Ueda. Randomly transitional phenomena in the system governed by Duffing's equation. *J. Statistical Physics* 20: 181-196, 1979.
24. K. Tomita. Periodically forced nonlinear oscillators. *Chaos*, ed. by A. V. Holden: 213-214. Manchester University Press, Manchester, 1986.
25. S. Kawamoto and T. Horiuchi. Algorithm for exact long time chaotic series and its application to cryptosystems. *I. J. of Bifurcation and Chaos* 14 (10): 3607-3611, 2004.
26. M. Hénon. A two-dimensional mapping with a strange attractor. *Communications in Mathematical Physics* 50: 69-77, 1976.
27. N. H. Tuan Anh, D. V. Liet and S. Kawamoto. Nonlinear dynamics of two-dimensional chaotic maps and fractal sets for snow crystals. *Handbook of Application of Chaos Theory*, ed. by C. H. Skiadas and C. Skiadas: 83-91. Chapman and Hall/CRC Press, 2016.